

# Satellites around Edge-on Galaxies. I. Dynamical Masses

D. V. Smirnov,<sup>1</sup> D. I. Makarov,<sup>2</sup> and I. D. Karachentsev<sup>2</sup>

<sup>1</sup>*Saint Petersburg State University, Saint Petersburg, 199034 Russia*

<sup>2</sup>*Special Astrophysical Observatory, Russian Academy of Sciences, Nizhnii Arkhyz, 369167 Russia\**

(Received May 30, 2023; Revised August 16, 2023; Accepted August 18, 2023)

We have undertaken a search for satellites around edge-on galaxies in the EGIPS catalog, which contains 16 551 objects with declinations above  $-30^\circ$ . We searched for systems with a central galaxy dominating in brightness by at least  $1^m$  compared to its companions. As a result, we discovered 1097 candidate satellites around 764 EGIPS galaxies with projected distances less than 500 kpc and a radial velocity difference less than  $300 \text{ km s}^{-1}$ . Of these, 757 satellites around 547 central galaxies have radial velocity accuracies higher than  $20 \text{ km s}^{-1}$  and satisfy the gravitationally bound condition. The ensemble of satellites is characterized by an average projected distance of 84 kpc and an average radial velocity dispersion of  $103 \text{ km s}^{-1}$ . Treating small satellites as test particles moving on isotropic orbits around central EGIPS galaxies, we determined the projected (orbital) masses of the edge-on galaxies. Within the luminosity range of  $1.3 \times 10^{10}$  to  $42 \times 10^{10} L_\odot$ , the total mass of the systems is well described by a linear dependence  $\log M_p \propto 0.88 \log \langle L_K \rangle_g$  with an average total mass-to- $K$ -band luminosity equal to  $(17.5 \pm 0.8) M_\odot/L_\odot$ , which is typical for nearby spiral galaxies such as the Milky Way, M 31 and M 81.

Keywords: galaxies: groups: general—galaxies: haloes—galaxies: spiral

## 1. INTRODUCTION

According to the  $\Lambda$ CDM standard cosmological model, the formation of galaxies in a diffuse medium takes place inside potential wells formed by fluctuations in the distribution of dark matter (Wechsler and Tinker, 2018). Only about 5% of the total density of the Universe is taken up by visible baryonic matter of galaxies (stars, gas and dust) (Aghanim et al., 2020). Traditional methods of determining the total mass of a galaxy, including the dark halo, from the rotation curve or from the stellar radial velocity dispersion (see, e.g., the survey by Zasov et al., 2017) are not sufficiently rigorous, since they imply an extrapolation of observational data far beyond the optical boundaries of the galaxy. Practically, two methods are suitable for direct estimation of the total mass: an analysis of the effects of weak gravitational lensing (e.g., Viola et al., 2015), which also requires a number of model assumptions, and an analysis of the kinematics of satellites surrounding the galaxy. Both methods have their advantages and shortcomings. The required accuracy of these methods is

reached by applying them to a large number of isolated galaxies, selected by morphological type or some other characteristics. The total masses of galaxies of various categories were determined from the kinematics of their satellites in many works: for spiral galaxies (Zaritsky et al., 1993, 1997; Zaritsky and White, 1994), for nearby galaxies of various types in the Local Volume (Karachentsev and Kudrya, 2014; Karachentsev and Kashibadze, 2021), for especially isolated galaxies (Karachentseva et al., 2021), and for thin late-type spirals seen edge-on (Karachentsev et al., 2016).

Karachentsev and Kudrya (2014) obtained a median estimate of the total (projected) mass-to- $K$ -band luminosity ratio of  $31 M_\odot/L_\odot$  considering the relative radial velocities and projected distances of satellites around 15 nearby galaxies similar to the Milky Way and Andromeda. Later Karachentsev and Kashibadze (2021) used a richer sample of 298 satellites around 25 bright Milky Way-type galaxies in the Local Volume and found for them an average ratio of  $\langle M_p/L_K \rangle = (31 \pm 6) M_\odot/L_\odot$ . Additionally, a higher  $M_p/L_K$  value was noted for a sample of 47 low-brightness galaxies similar to the neighboring M 33 galaxy and the Magellanic Clouds. The average  $M_p/L_K$  ratio for the disk-

\*Electronic address: dim@sao.ru

dominated galaxies,  $(17.4 \pm 2.8) M_{\odot}/L_{\odot}$ , turned out to be significantly lower than for the bulge-dominated galaxies,  $(73 \pm 15) M_{\odot}/L_{\odot}$ .

Karachentseva et al. (2021) used a similar approach for estimating the total masses of particularly isolated galaxies. Based on the radial velocities and projected distances of 141 satellites, they obtained  $\langle M_p/L_K \rangle = (20.9 \pm 3.1) M_{\odot}/L_{\odot}$ , noting the upward trend of this ratio towards earlier-type galaxies.

An independent determination of  $M_p/L_K$  for Sc–Sd galaxies was carried out by Karachentsev and Karachentseva (2019). An average ratio of  $(20 \pm 3) M_{\odot}/L_{\odot}$  was obtained from 43 satellites for 220 galaxies without visible bulges and oriented face on, which is in agreement with the previous estimates.

In this work we consider the kinematics of satellites that we discovered around edge-on galaxies in the EGIPS catalog (Makarov et al., 2022). Edge-on galaxies attract our attention by the fact that such an orientation gives one an opportunity to investigate directly the distribution of satellites with respect to the disk plane of the galaxies, which is impossible in other scenarios. The EGIPS catalog is the largest sample of edge-on galaxies to date, which allows one to significantly increase the statistics and, as a consequence, enhance the reliability of the obtained results. In this work we use the standard cosmological  $\Lambda$ CDM model with parameters  $H_0 = 72.0 \text{ km s}^{-1} \text{ Mpc}^{-1}$ ,  $\Omega_m = 0.3$ ,  $\Omega_{\Lambda} = 0.7$ .

## 2. SATELLITE SAMPLING

The sample of central objects is based on the new catalog of edge-on galaxies (EGIPS, Makarov et al., 2022), discovered in the images of the Pan-STARRS1 DR2(PS1, Chambers et al., 2016) survey. It contains data on 16 551 galaxies located above  $\delta > -30^{\circ}$ . The photometry that we carried out using the **SExtractor** (Bertin and Arnouts, 1996) package in all five filters ( $g$ ,  $r$ ,  $i$ ,  $z$ ,  $y$ ) of the PS1 survey provides an unbiased flux estimate with an accuracy of about 0.05 for galaxies fainter than  $r \simeq 13^{\text{m}}8$ . Most EGIPS galaxies (about 63%)

have redshift measurements with a median value of  $cz_{\text{CMD}} \approx 12\,000 \text{ km s}^{-1}$ , corresponding to a depth of about 170 Mpc. To avoid uncertainties in the galaxy distance estimates due to high peculiar velocities in the nearby Universe, we restricted our study to EGIPS galaxies with  $cz_{\text{LG}} \geq 2000 \text{ km s}^{-1}$ . Due to observational selection the number of galaxies with known redshifts falls drastically after  $cz_{\text{CMD}} \approx 12\,000 \text{ km s}^{-1}$ . Statistics are extremely sparse for systems with redshifts above  $30\,000 \text{ km s}^{-1}$  (there are about 10 systems with higher velocities), and we therefore limited the sample by a maximum redshift of  $cz_{\text{CMD}} = 30\,000 \text{ km s}^{-1}$ .

The sample of candidate satellites was formed in four stages. The first step consisted of compiling a list of approximately 3.2 million galaxies with known redshifts and photometry from SDSS DR17 (Abdurro’uf et al., 2022) survey data and the HyperLeda<sup>1</sup> (Makarov et al., 2014) database. The use of SDSS provides highly homogeneous data; however, it presents a number of difficulties. For a large number of bright galaxies ( $m_r \lesssim 14^{\text{m}}5$ ) that fall into the photometric part of the SDSS survey, no radial velocity or magnitude measurements were carried out. Additionally, there is the well-known problem of “splitting” of the images of nearby galaxies into several objects, which leads to two interrelated effects: underestimated luminosity of the galaxy on the one hand, and obtaining the spectrum of the galaxy away from its physical center on the other hand, which introduces an error into the redshift measurements of the galaxies. Using HyperLeda data allows one to solve the problem of bright galaxies. Accurate integral photometry is available for most of them, and redshift data is no less than 96% complete for galaxies with  $B \leq 15^{\text{m}}5$  (Falco et al., 1999). Additionally, HyperLeda contains a large collection of data obtained in the course of mass neutral hydrogen line sky surveys, such as ALFALFA (Haynes et al., 2018) and HIPASS (Meyer et al., 2004).

Before starting the selection procedure, we transformed the inhomogeneous galaxy photometric data from different surveys to a sin-

<sup>1</sup> <https://leda.univ-lyon1.fr/>

gle  $K_s$ -band magnitude in the 2MASS photometric system (Skrutskie et al., 2006). The choice of this filter is due to a close relation of the  $K$ -luminosity of the stellar population of galaxies with their total stellar mass. Galaxies brighter than  $K_s < 13^m5$  usually have original flux measurements in the 2MASS survey. HyperLeda data were therefore used without any transformation for galaxies with known  $K$ -photometry. The overwhelming majority of our sample galaxy data were obtained from the SDSS survey. In order to convert the SDSS-magnitudes to the 2MASS system we used the following expression:

$$(g - K_s)_0 = 1.907(g - r)_0 + 1.654(r - i)_0 + 0.684 \quad (1)$$

with a standard deviation  $\sigma = 0.126$  (Bilir et al., 2008, equation (15)). A detailed inspection of the galaxies in the final sample revealed the fact that the SDSS-photometry for some of them, usually for chunky and extended LSB-galaxies, is obviously erroneous. In these cases we used the  $g$ -,  $r$ - and  $z$ -band photometry from DESI Legacy Surveys (Dey et al., 2019), unifying three projects: the Dark Energy Camera Legacy Survey (DECaLS), the Beijing-Arizona Sky Survey (BASS), and the Mayall  $z$ -band Legacy Survey (MzLS). To estimate the  $K_s$ -magnitude from these data, we operated in steps. First, Legacy photometry was converted to the SDSS system in the assumption that  $r - i \approx i - z \approx 0^m15$ , typical for late-type galaxies at  $z = 0$  (Fukugita et al., 1995; Shimasaku et al., 2001), and then to the 2MASS system, using equation (1). For the DECaLS survey data, we used the B1 conversion equations from Abbott et al. (2021), and for the BASS and MzLS survey, those from Zou et al. (2019). As mentioned above, photometry for galaxies from the EGIPS catalog was carried out in the PS1 system. EGIPS galaxy magnitudes in the SDSS system were derived from the conversion equations of Tonry et al. (2012) and were afterwards converted to  $K_s$  by formula (1). Note that the final sample contains original 2MASS photometry for the vast majority of the central EGIPS galaxies (we had to use optical photometry only for 28 out of 764 objects). In the case of candidate satellites,  $K$ -magnitudes were esti-

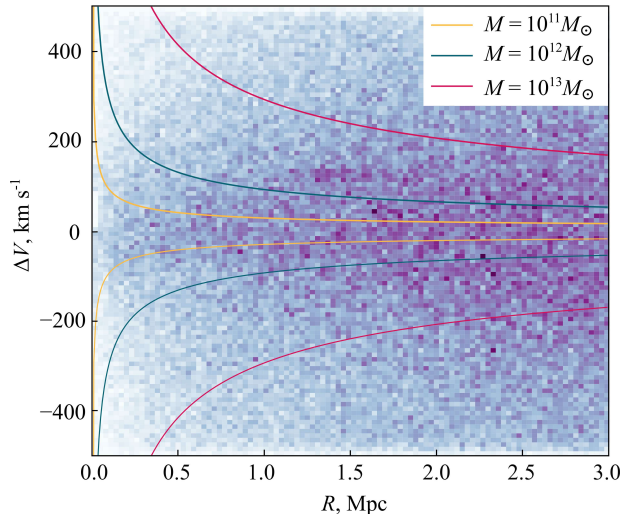


**Figure 1:** Distribution of neighboring galaxies in the  $(\Delta V, R)$  plane. The colored lines show the escape velocity curves for different point masses.

mated from the conversion equations for 60% of the galaxies. However, this should not lead to a significant luminosity underestimation, since the satellite sample is based on dwarf galaxies, where the influence of internal extinction is small. All photometric data were corrected for Galactic extinction using the calibration from Schlafly and Finkbeiner (2011).

As the next step, a list of neighbors was compiled for each galaxy in the EGIPS catalog. It included all galaxies within a projected distance of less than 3 Mpc and with a velocity difference no greater than  $500 \text{ km s}^{-1}$  with respect to the edge-on galaxy. The SDSS object selection algorithm often leads to artificial splitting of extended and clumpy galaxies into a large number of pseudo galaxies. For some of these pseudo galaxies spectra and redshifts were obtained within the SDSS framework, reflecting, rather, the kinematics of the galaxy itself and not its satellites. In order to avoid the inclusion of these pseudo galaxies in the lists of neighbors, we excluded from consideration all objects falling into the  $r$ -band Petrosian ellipse of the EGIPS galaxy (if the  $r$ -band photometry was of poor quality, we used data in other bands, primarily  $g$ ). Figure 1 shows the distribution of neighboring galaxies on the  $(\Delta V, R)$  plane, where  $\Delta V = (V_{\text{neighbour}} - V_{\text{EGIPS}})/(1 + z)$  is the

cosmologically corrected neighbor velocity with respect to the EGIPS galaxy, and  $R$  is the projected distance between the neighbor galaxy and the edge-on galaxy. As is evident from the figure, the filling of the plane is approximately homogeneous at large projected distances ( $R \gtrsim 1.5$  Mpc), and a rather pronounced concentration of neighbors is observed near  $\Delta V = 0$ . At this stage, we removed all EGIPS galaxies containing a brighter companion at a projected distance less than 1.5 Mpc and with a radial velocity difference smaller than the escape velocity, which corresponds to a point mass of  $M = 10^{13} M_{\odot}$ . The aim of this step is to exclude from consideration galaxies that are part of groups with a more massive companion, and to separate the EGIPS galaxy satellites from members of groups where the edge-on galaxy is not the dominating galaxy in terms of mass.

To form a list of possible satellites for the considered galaxies, we selected all objects with  $|\Delta V| \leq 300 \text{ km s}^{-1}$  and  $R < 0.5$  Mpc, which roughly corresponds to the parameters of the known groups of galaxies. However, in this case we still consider galaxies with companions of comparable luminosity—pairs like the Milky Way and Andromeda. Due to projection effects, the task of isolating satellites of specific galaxies is also very complicated in such systems. We therefore excluded from the sample EGIPS galaxies with companions within 0.5 Mpc, imposing an absolute magnitude condition  $(M^K - M_{\text{EGIPS}}^K) \leq 1^{\text{m}}$ . At this stage, we effectively selected isolated groups of galaxies where the central galaxy, seen edge-on, dominates in luminosity over its neighbors by a factor of at least 2.5.

Ideally, the used approach allows one to select isolated systems with a galaxy dominating in luminosity and its satellites. However, during visual inspection we discovered that in some cases the algorithm leaves for consideration galaxies that are probably members of clusters or groups with a neighbor of comparable mass. This is due to the incompleteness of redshift data for galaxies or to the location of the considered system at the periphery of a dynamically hot cluster. To clean the sample from such contamination, we looked over all galaxies remaining at

this stage and excluded from consideration the ones with a high probability of being members of clusters or large groups. In total, 19 candidates were excluded around 14 EGIPS galaxies; a description of every such case is presented in Appendix A. We also excluded from consideration two EGIPS galaxies: EGIPS J144339.4+110821 and EGIPS J131905.6–242504. In the first case, no adequate photometry is available for the galaxy, and in the second—clear signs of interaction are visible, distorting the velocity measurements for the galaxy.

As a result of the procedure sequence described above, we are left with 764 EGIPS galaxies and 1097 candidate satellites. The data on these objects are presented in the Table 1 (the full version is available online).

Figure 2 shows the distributions of the central galaxies and their candidate satellites by luminosity and redshift. The separation of central galaxies into the red and blue ones was carried out according to the condition  $(g - i)_0 \leq 0.91$ , which allows one to adequately separate the galaxies of the “red sequence” from those of the “blue cloud” (Makarov et al., 2022). The distribution of central red galaxies is characterized by a median  $K$ -luminosity of  $\widetilde{M}_K = -24^{\text{m}}3$ , and that of the candidate satellites— $\widetilde{M}_k = -21^{\text{m}}2$ . For central galaxies of the “blue cloud” the median luminosity is equal to  $\widetilde{M}_K = -22^{\text{m}}1$ , and for their satellites— $\widetilde{M}_k = -19^{\text{m}}2$ .

Figure 3 shows the distribution of all 1097 candidate satellites for the red and blue EGIPS galaxies in the  $(\Delta V, R)$  plane. The radial velocity of most of the candidates differs from the velocity of the central galaxy by less than  $100 \text{ km s}^{-1}$ , which is expected for gravitationally bound systems around isolated massive galaxies like the Milky Way.

### 3. SELECTION OF GRAVITATIONALLY BOUND SATELLITES

For a more detailed filtering of the background galaxies, we used a technique proposed and developed in the works dedicated to the study of galaxy groups on a scale of up to  $z \sim 0.01$  (Karachentsev and Makarov, 2008;

**Table 1:** Candidate satellites for EGIPS galaxies. The following parameters are listed in the columns: (1) and (2) give the name of the candidate according to the HyperLeda (Makarov et al., 2014) database and the J2000.0 coordinates of the candidate; (3) and (4) present the redshift of the candidate in the cosmic microwave background reference frame in  $\text{km s}^{-1}$  and the redshift error; (5)–(8) give the total  $g$ ,  $r$ ,  $i$ -band magnitudes of the candidates in the SDSS photometric system and the  $K_{s0}$  magnitudes of the 2MASS system. These magnitudes are corrected for Galactic extinction according to Schlafly and Finkbeiner (2011); (9) gives the absolute  $K_s$  magnitude of the candidate; (10) and (11) contain the name of the central EGIPS galaxy and its coordinates according to Makarov et al. (2022); (12) gives the redshift of the central galaxy in the cosmic microwave background system; (13) and (14) contain the angular and projected distances between the candidate and the central galaxy in arcminutes and kpc correspondingly; (15) gives the radial velocity difference corrected for cosmological expansion  $\Delta V = (V_{\text{candidate}} - V_{\text{EGIPS}})/(1+z)$ ; (16) and (17) contain the numeric values for the escape velocity (equation (4)) and turnaround radius (equation (5)) selection criteria, correspondingly. A sample is shown; the full version is available as online supplementary material.

No	Candidate	J2000.0	$cz_{\text{CMB}}$	$e_{cz}$	$g_0$	$r_0$	$i_0$	$K_{s0}$	$M_K$
	(1)	(2)	(3)	(4)	(5)	(6)	(7)	(8)	(9)
1	SDSS J000043.54+143129.5	J000043.5+143130	27892.2	10.0	18.69	17.75	17.75	15.5	−22.58
2	UGC12895	J000038.4+200333	6394.4	2.9	15.86	15.49	15.49	14.1	−20.68
3	[MKB2002]J000409.64+042553.3	J000409.6+042551	11488.6	60.0	18.01	17.66	17.66	16.28	−19.79
4	AGC102304	J000510.6+050954	7852.1	6.2	17.77	17.43	17.43	16.11	−19.12
5	PGC000425	J000556.1−135846	5585.2	70.0				14.05	−20.43
6	SDSS J000634.50−004714.2	J000634.5−004714	12677.4	3.7	19.57	19.28	19.28	18.1	−18.2
7	AGC105303	J000922.2+104104	6076.2	6.1	16.38	15.92	15.92	14.4	−20.27
8	PGC001031	J001524.4+184624	5215.8	8.5				11.75	−22.58
9	PGC1146389	J001529.0−001854	17771.7	2.7	17.2	16.76	16.76	15.19	−21.87
10	SDSS J001610.69−011244.9	J001610.7−011245	24925.4	2.1	18.78	18.11	18.11	16.11	−21.71

No	EGIPS ID	J2000.0	$cz_{\text{CMB}}$	$R$ , arcmin	$R$ , kpc	$\Delta V$	$f_{V_{\text{esc}}}$	$f_{R_{\text{ta}}}$
	(10)	(11)	(12)	(13)	(14)	(15)	(16)	(17)
1	J000042.1+143023	J000042.2+143023	27841.1	1.16	118.0	46.7	0.15	0.01
2	J000055.9+202017	J000056.0+202017	6451.5	17.24	461.0	−55.9	2.42	2.1
3	J000344.7+041753	J000344.8+041753	11205.0	10.08	449.4	273.4	26.55	0.92
4	J000506.6+051213	J000506.6+051213	7695.0	2.52	79.5	153.1	1.97	0.01
5	J000556.8−135944	J000556.8−135945	5411.4	0.99	22.6	170.8	1.76	0.0
6	J000628.8−004702	J000628.9−004703	12907.3	1.43	72.5	−220.4	3.36	0.0
7	J000904.2+105508	J000904.2+105508	6324.9	14.74	387.4	−243.5	25.52	0.83
8	J001440.0+183455	J001440.1+183455	5055.3	15.56	332.3	157.8	4.5	0.26
9	J001539.8−001601	J001539.8−001601	17613.9	3.96	267.7	149.0	8.37	0.35
10	J001615.2−011213	J001615.3−011214	24839.7	1.26	115.7	79.2	0.49	0.01

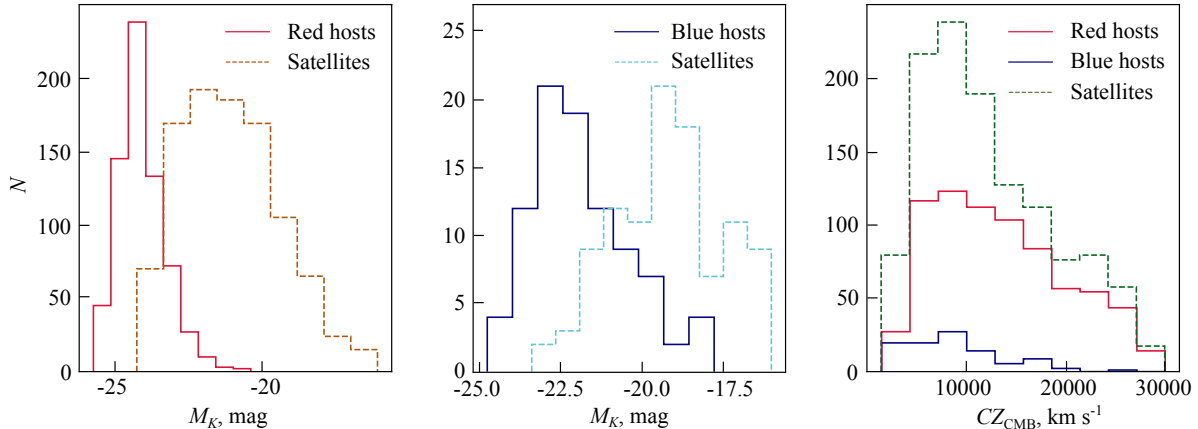


**Figure 2:** Histograms of the distribution of central EGIPS galaxies and candidate satellites by absolute  $K$ -band magnitude ((a) for systems with red central galaxies, (b) blue central galaxies) and redshift (c).

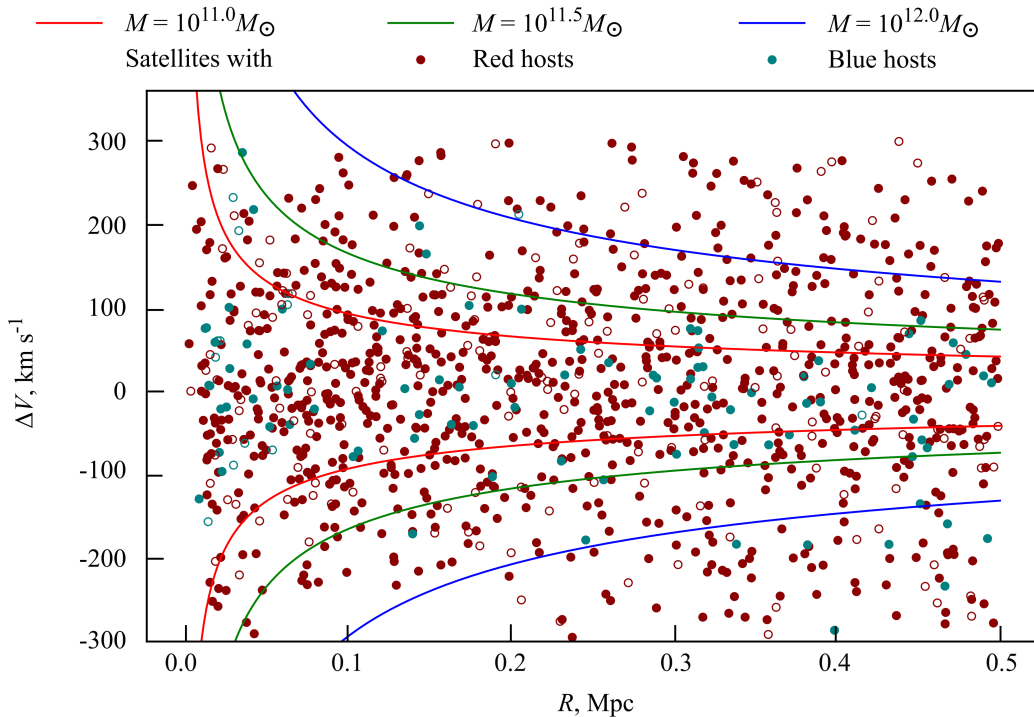


**Figure 3:** Distribution of candidate satellites on the  $(\Delta V, R)$  plane. The colored lines show the escape velocity curves for different central point masses. The empty circles show galaxies with velocity measurement errors  $e_{cz} \leq 20 \text{ km s}^{-1}$ .

Makarov and Karachentsev, 2011, 2009). A physical pair of galaxies should satisfy a series of restrictions. Evidently, the total energy of a bound system should be negative, from where it follows that the mutual velocity of the galaxies should be lower than the escape velocity in a gravitating system,  $v^2 < v_{\text{esc}}^2 = 2GM/r$ . Since

the observed radial velocity difference,  $\Delta V$ , and the projected distance between the galaxies,  $R$ , are obviously smaller than their spatial counterparts ( $v$  and  $r$  correspondingly), then this relation between the observed parameters becomes

even stricter:

$$\Delta V^2 < v^2 < 2\frac{GM}{r} < 2\frac{GM}{R}. \quad (2)$$

Additionally, the “zero-velocity sphere” radius, also called the turnaround radius, determines the boundary between the already collapsed high-density region and the Universe with on-going expansion:

$$r_{\text{ta}}^3 \simeq \frac{8GM}{\pi^2 H_0^2}. \quad (3)$$

This places a natural limit on the maximum linear size of the system.

Assuming the relation  $M = \kappa L_K$  between the total mass of a gravitating system and its luminosity, we can rewrite the conditions described above in terms of the “mass-to-luminosity” ratio. For a physical system, the projected “mass-to-luminosity” ratio for the escape velocity (equation (2)) gives

$$\frac{\Delta V^2 R}{2G(L_{\text{host}} + L_{\text{sat}})} < \kappa, \quad (4)$$

and from the turnaround radius condition (3) we get

$$\frac{\pi^2 R^3 H_0^2}{8G(L_{\text{host}} + L_{\text{sat}})} < \kappa, \quad (5)$$

where  $L_{\text{host}}$  and  $L_{\text{sat}}$  denote the  $K$ -luminosity of the central galaxy and its satellite, correspondingly. Figure 4 shows the distributions of candidate satellites by the projected “mass-to-luminosity” ratios for the escape velocity and turnaround radius. We limited the satellite sample assuming the value  $\kappa = 9 M_\odot/L_\odot$  for both ratios.

As was noted by Makarov and Karachentsev (2011), the redshift measurement errors may introduce a substantial contribution to the velocity dispersion of galaxies in groups, especially when these errors turn out to be comparable with the expected velocity dispersion for the satellites, approximately or less than  $100 \text{ km s}^{-1}$ . As is evident from Fig. 5, for most of the candidates the radial velocity measurement error does not exceed  $20 \text{ km s}^{-1}$ . A selection of precisely such galaxies, therefore, became the finishing touch in

our sampling of satellites around edge-on galaxies. The final sample for analysis of the kinematics of groups with a central luminosity dominant galaxy consists of 757 satellites around 547 EGIPS galaxies.

#### 4. SYSTEM MASS ESTIMATION

The average number of candidate satellites per host galaxy in the resulting sample does not exceed one and a half. This makes the determination of masses of individual EGIPS galaxies very unreliable. We assumed that the central galaxies of comparable luminosities have roughly equal masses, and therefore, kinematics of the surrounding satellites. Therefore, for estimating system masses, we decided not to consider individual galaxies but assemble groups consisting of all candidate satellites around EGIPS galaxies of similar luminosity. We divided our sample into 10 subsamples based on the luminosity of the host EGIPS galaxy. An approximate equality of the number of candidate satellites in each subsample was the main criterion of the division. Unfortunately, the luminosity range covered by the subsamples of the brightest host galaxies turned out to be too wide. Two subsamples with a somewhat smaller number of objects were formed from EGIPS galaxies with  $L_K \geq 2.14 \times 10^{11} L_\odot$  for further refinement. Figure 6 shows the distribution of the candidate satellites for each of the 10 subsamples, divided according to the luminosity of the host EGIPS galaxy. Each such subsample was considered from this point on as a single composite system of satellites.

Owing to the candidate selection algorithm for each assembled group described above, the luminosity and mass of the satellites turned out to be significantly lower than those of the host galaxy. We can therefore use a simplification for estimating group masses, which views satellites as test particles moving in the gravitational field of the central galaxy. Bahcall and Tremaine (1981) emphasized the problems with using the virial theorem: the mass estimate with account for projection effects turns out to be biased, statistically ineffective and inconsistent. They sug-

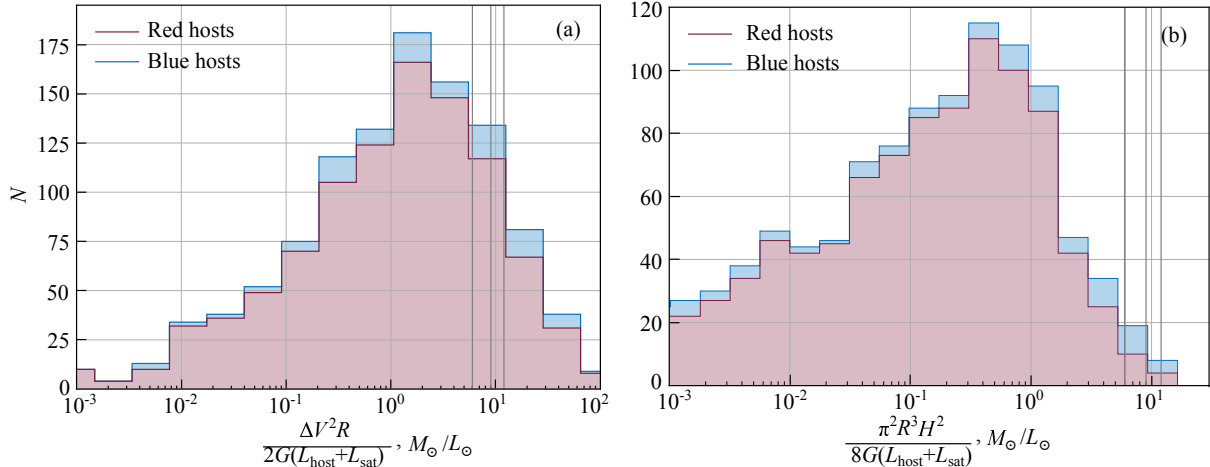


**Figure 4:** Cumulative histograms of the distribution of candidate satellites by “virial” (a) and “spatial” parameters (b). The vertical lines correspond to the “mass-to-luminosity” ratios  $\kappa = 6, 9, 12 M_{\odot}/L_{\odot}$ .

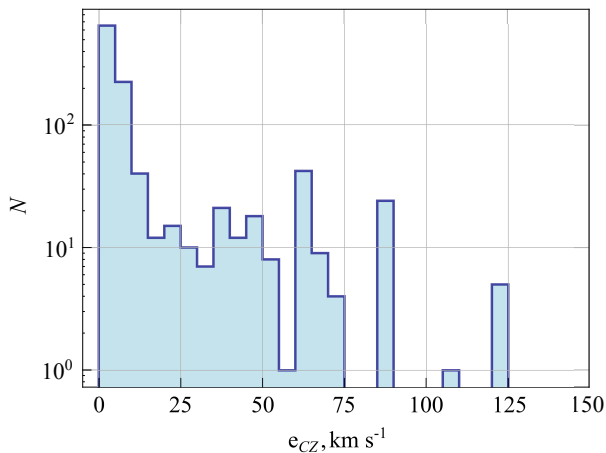


**Figure 5:** Distribution of candidate satellites by radial velocity errors. The number of galaxies is presented in logarithmic scale for better visualization of the distribution.

gested an alternative to the virial theorem—a projected mass estimator free of these shortcomings. Unfortunately, the projected mass estimator depends on the shape of the orbit of the moving particles. An assumption of isotropic orbits with an average squared eccentricity equal to  $\langle e^2 \rangle = 1/2$  seems most natural. In this case, the projected mass estimator becomes (Bahcall

and Tremaine, 1981, eq. (20))

$$M_p = \frac{16}{\pi G N} \sum_{i=1}^N \Delta V_i^2 R_i. \quad (6)$$

Unlike the virial theorem, where the projection effects make the mass estimate statistically ineffective, the dispersion of the projected mass estimate is clearly defined and, in the case of isotropic orbit distribution, is equal to (Bahcall and Tremaine, 1981, eq. (22)):

$$\sigma^2(M_p) = \frac{1}{N} \left( \frac{128}{5\pi^2} - 1 \right) \langle M_p \rangle^2. \quad (7)$$

We used these relations to estimate the assembled group masses and their errors.

The average properties of the central galaxies and the corresponding assembled groups are summarized in Table 2. Besides the assembled groups with designations from  $L_1$  to  $L_{10}$ , it gives the mean parameters for the total sample of central galaxies, as well as separately for the “blue” galaxy subsample.

As is evident from the data in the last column of Table 2 and Fig. 6, the distribution of satellite velocities with respect to the central galaxies turns out to be statistically unbiased.

There is a close correlation between the total luminosity of an assembled group and its



**Table 2:** Main parameters of the samples under consideration. The  $M_p$  values are computed for the limit  $\kappa \leq 9$  and  $e_{cz} \leq 20 \text{ km s}^{-1}$ . The following data are given in the columns for each system: (1) subsample name; (2)—number  $N_{\text{host}}$  of central EGIPS galaxies assembled in a group; (3)  $K$ -luminosity range covered by the given subsample; (4) average  $K$ -luminosity of the central galaxies  $\langle K \rangle_{\text{h}}$ ; (5) average  $\langle cz \rangle$  and (6) median  $\tilde{cz}$  redshift in the cosmic microwave background reference frame for the subsample of central galaxies; (7) number of satellites  $N_{\text{sat}}$  in the assembled group; (8) satellite velocity scattering relative to the central galaxy,  $\sigma^2 = \sum \Delta V_i^2 / N_{\text{sat}}$ , where the velocity difference  $\Delta V$  is corrected for cosmological expansion  $1/(1+z)$ ; (9) harmonic mean for the projected distances of the satellites from the host galaxy  $R_{\text{harm}} = 1/\langle 1/R \rangle$ ; (10) averaged total luminosity of the group with account for the contribution from the satellites  $\langle L_K \rangle_{\text{g}}$ ; (11) estimate of the projected mass  $M_p$  of the system, derived from equation (6); (12) “mass-to-luminosity” ratio  $M_p/L_K$ ; (13) systemic difference of the mean satellite system velocity with respect to the central galaxy  $\langle \Delta cz \rangle$

Name	$N_{\text{host}}$	$L_K$ -range, $10^9 L_{\odot}$	$\langle L_K \rangle_{\text{h}}$ , $10^9 L_{\odot}$	$\langle cz \rangle$ , $\text{km s}^{-1}$	$\tilde{cz}$ , $\text{km s}^{-1}$	$N_{\text{sat}}$	$\sigma$ , $\text{km s}^{-1}$	$R_{\text{harm}}$ , kpc	$\langle L_K \rangle_{\text{g}}$ , $10^9 L_{\odot}$	$M_p$ , $10^{11} M_{\odot}$	$M_p/L_K$ , $M_{\odot}/L_{\odot}$	$\langle \Delta cz \rangle$ , $\text{km s}^{-1}$
(1)	(2)	(3)	(4)	(5)	(6)	(7)	(8)	(9)	(10)	(11)	(12)	(13)
Full	547		114.0	12861	11605	757	103	84	132.5	$23.2 \pm 1.1$	17.5	$0 \pm 4$
$L_1$	36	0.28–22.5	12.1	7037	6237	38	47	33	13.3	$2.89 \pm 0.59$	21.7	$-10 \pm 8$
$L_2$	67	22.5–46.5	35.7	9061	8251	82	66	70	39.4	$6.67 \pm 0.93$	16.9	$0 \pm 7$
$L_3$	76	46.5–70	58.6	10714	9892	91	90	77	66.2	$12.3 \pm 1.6$	18.6	$6 \pm 10$
$L_4$	66	70–93	81.5	10554	9938	96	96	83	92.8	$17.4 \pm 2.2$	18.8	$3 \pm 10$
$L_5$	71	93–113	103.1	12467	12238	94	106	100	117.8	$20.3 \pm 2.6$	17.2	$7 \pm 11$
$L_6$	68	113–136	125.0	14076	14216	92	118	75	145.5	$27.9 \pm 3.7$	19.2	$-15 \pm 12$
$L_7$	55	136–166	151.6	14618	14587	88	114	107	179.2	$29.8 \pm 4.0$	16.6	$3 \pm 12$
$L_8$	51	166–214	188.0	15976	17311	77	108	143	222.4	$31.5 \pm 4.5$	14.2	$9 \pm 12$
$L_9$	38	214–300	246.1	17254	19521	62	118	123	285.3	$35.4 \pm 5.7$	12.4	$-7 \pm 15$
$L_{10}$	19	300–440	346.2	18485	20118	37	140	119	415.3	$64.3 \pm 13.3$	15.5	$-11 \pm 23$
Blue	48		29.7	10120	9289	51	64	52	34.0	$7.6 \pm 1.3$	22.5	$-9 \pm 9$

projected mass, shown in Fig. 7. The interrelation between mass and  $K$ -luminosity is well-described by a linear dependence in logarithmic scales

$$\log M_p = (0.875 \pm 0.028) \log \langle L_K \rangle_{\text{g}} + (2.59 \pm 0.29). \quad (8)$$

The slope of the dependence at a  $4\sigma$  level is less than one.

## 5. CONCLUDING STATEMENTS

Using photometry and redshifts obtained in the SDSSDR17 (Abdurro’uf et al., 2022) survey and collected in the HyperLeda (Makarov

et al., 2014) database, we carried out a search for possible satellite candidates around edge-on galaxies from the EGIPS (Makarov et al., 2022) catalog. We searched for systems with a central luminosity dominant galaxy:  $(M^K - M_{\text{EGIPS}}^K) > 1^{\text{m}}$ . We found 1097 candidate satellites around 764 EGIPS galaxies with radial velocities in the range of  $cz_{\text{LG}} \geq 2000$  and  $cz_{\text{CMD}} \leq 30000 \text{ km s}^{-1}$  with projected distances of less than 500 kpc and radial velocities of less than  $300 \text{ km s}^{-1}$  with respect to the central galaxy. Out of these, 757 satellites around 547 central galaxies have redshift accuracies better than  $20 \text{ km s}^{-1}$  and satisfy the criterion of a gravitationally bound system, which

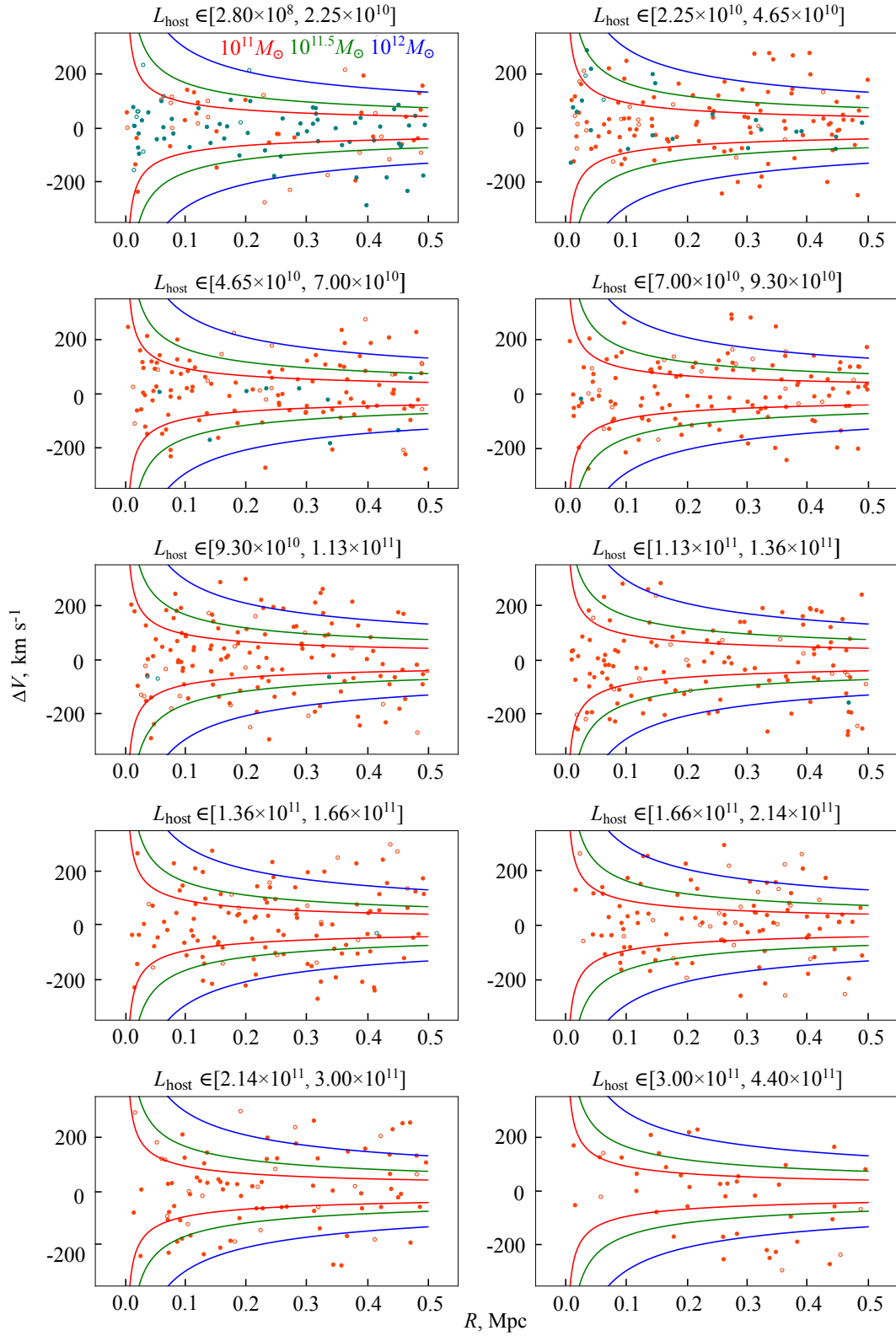


**Figure 6:** Distribution of candidate satellites in the  $(\Delta V, R)$  plane, divided into subsamples according to the luminosity of the host galaxy. The designations are the same as in Fig. 3.

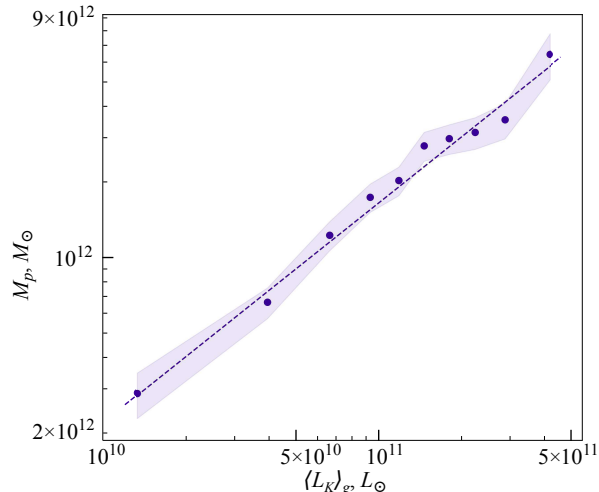


**Figure 7:** The dependence of assembled group mass on luminosity. The linear regression from equation (8) is shown by the dashed line. The shaded regions mark the  $1\sigma$  interval of the mass estimate errors.

makes them suitable for determining the physical parameters of the systems. The population of satellites has a typical projected distance of 84 kpc and a mean velocity dispersion of  $103 \text{ km s}^{-1}$ . The distribution of satellite velocities relative to the central galaxies is statistically unbiased. Assuming an isotropic nature of the satellite orbits with an average eccentricity of  $\langle e^2 \rangle = 1/2$ , we estimated the total (projected) masses of EGIPS galaxies. In a wide interval of luminosities the projected mass estimates for the EGIPS galaxies follow the dependence  $M_p \propto \langle L_K \rangle_g^{0.88}$  with an average ratio  $(17.5 \pm 0.8) M_\odot / L_\odot$ , typical for nearby massive spiral galaxies (Karachentsev and Kashibadze, 2021; Karachentsev and Kudrya, 2014). Numerous works dedicated to studying galaxy groups have revealed that the “mass-to-luminosity” ratio of the systems increases with luminosity and mass. Thus, Makarov and Karachentsev (2011) used a sample of approximately 11 thousand galaxies on the scale of the Local Supercluster  $cz_{LG} \leq 3500 \text{ km s}^{-1}$  to find the dependence  $M \propto L_K^{1.15}$ . In that work, the overwhelming majority are groups with luminosity  $L_K \gtrsim 10^{10} L_\odot$  and a median  $L_K = 1.2 \times 10^{11} L_\odot$ . However, when switching to systems of lower luminosities, the behavior of the dependence changes

dramatically. In their studies of dwarf galaxies, Tully (2005) and Tully et al. (2006) discovered that low luminosity groups demonstrate a significantly higher “mass-to-luminosity” ratio compared to the “normal” groups. A similar result was obtained by Makarov and Uklein (2012). Kourkchi and Tully (2017) postulated the dependence  $M/L_K \propto L_K^{-0.5}$  for systems with luminosities  $L_K < 9.27 \times 10^8 L_\odot$ . In their studies of the nearby groups of galaxies at distances less than 11 Mpc in the Local Volume, probably the most studied region of the Universe, Karachentsev and Kashibadze (2021) have shown that low luminosity groups are well-described by this dependence. The transition between the dependences for groups of low and high luminosity takes place at  $L_K \simeq 3 \times 10^{10} L_\odot$ . The “mass-to-luminosity” ratio near this luminosity reaches its maximum value, which indicates the most effective transformation of matter into stars for systems of this luminosity. The central dominating galaxies of the groups in our work occupy precisely the luminosity range falling into the transition zone. Expression (8) and Table 2 demonstrate a gradual growth of the “mass-to-luminosity” ratio into the region of low luminosity galaxies.

As the next stage of our work we propose investigating the orientation and nature of the satellite motion with account for the direction of rotation of the EGIPS galaxies themselves. This task became relevant lately due to the discovery of planar structures of the satellites around the Milky Way, Andromeda, and other massive nearby galaxies (Kroupa et al., 2005; Koch and Grebel, 2006; Ibata et al., 2013; Pawlowski et al., 2015; Tully et al., 2015; Libeskind et al., 2019; Martínez-Delgado et al., 2021), being a serious challenge for the standard cosmological model on the scale of the order of 100 kpc.

## ACKNOWLEDGMENTS

We are grateful to the referee for valuable comments that helped us significantly improve the paper. We acknowledge the usage of the HyperLeda database (<https://leda.univ-lyon1.fr/>). Funding for the Sloan Digital Sky Survey V has been provided by the Al-

fred P. Sloan Foundation, the Heising-Simons Foundation, the National Science Foundation, and the Participating Institutions. SDSS acknowledges support and resources from the Center for High-Performance Computing at the University of Utah. The SDSS web site is [www.sdss.org](http://www.sdss.org). SDSS is managed by the Astrophysical Research Consortium for the Participating Institutions of the SDSS Collaboration, including the Carnegie Institution for Science, Chilean National Time Allocation Committee (CNTAC) ratified researchers, the Gotham Participation Group, Harvard University, Heidelberg University, The Johns Hopkins University, L'École polytechnique fédérale de Lausanne (EPFL), Leibniz-Institut für Astrophysik Potsdam (AIP), Max-Planck-Institut für Astronomie (MPIA Heidelberg), Max-Planck-Institut für Extraterrestrische Physik (MPE), Nanjing University, National Astronomical Observatories of China (NAOC), New Mexico State University, The Ohio State University, Pennsylvania State University, Smithsonian Astrophysical Observatory, Space Telescope Science Institute (STScI), the Stellar Astrophysics Participation Group, Universidad Nacional Autónoma de México, University of Arizona, University of Colorado Boulder, University of Illinois at Urbana-Champaign, University of Toronto, University of Utah, University of Virginia, Yale University, and Yunnan University.

## FUNDING

This work was carried out with the financial support of the RSF grant No. 19-12-00145.

## CONFLICT OF INTEREST

The authors declare no conflict of interest regarding the publication of this paper.

## REFERENCES

T. M. C. Abbott, M. Adamów, M. Aguena, et al., *Astrophys. J. Suppl.* **255** (2), id. 20 (2021).  
 Abdurro'uf, K. Accetta, C. Aerts, et al., *Astrophys. J. Suppl.* **259** (2), id. 35 (2022).

N. Aghanim et al. (Planck Collab.), *Astron. and Astrophys.* **641**, id. A6 (2020).  
 J. N. Bahcall and S. Tremaine, *Astrophys. J.* **244**, 805 (1981).  
 E. Bertin and S. Arnouts, *Astron. and Astrophys. Suppl.* **117**, 393 (1996).  
 M. Bilicki, T. H. Jarrett, J. A. Peacock, et al., *Astrophys. J. Suppl.* **210** (1), article id. 9 (2014).  
 S. Bilir, S. Ak, S. Karaali, et al., *Monthly Notices Royal Astron. Soc.* **384** (3), 1178 (2008).  
 K. C. Chambers, E. A. Magnier, N. Metcalfe, et al., arXiv e-prints astro/ph:1612.05560 (2016).  
 A. Dey, D. J. Schlegel, D. Lang, et al., *Astron. J.* **157** (5), article id. 168 (2019).  
 E. E. Falco, M. J. Kurtz, M. J. Geller, et al., *Publ. Astron. Soc. Pacific* **111** (758), 438 (1999).  
 M. Fukugita, K. Shimasaku, and T. Ichikawa, *Publ. Astron. Soc. Pacific* **107**, 945 (1995).  
 M. P. Haynes, R. Giovanelli, B. R. Kent, et al., *Astrophys. J.* **861** (1), article id. 49 (2018).  
 P. Hickson, *Astrophys. J.* **255**, 382 (1982).  
 R. A. Ibata, G. F. Lewis, A. R. Conn, et al., *Nature* **493** (7430), 62 (2013).  
 I. Karachentsev and O. Kashibadze, *Astronomische Nachrichten* **342** (999), 999 (2021).  
 I. D. Karachentsev and V. E. Karachentseva, *Monthly Notices Royal Astron. Soc.* **486** (3), 3697 (2019).  
 I. D. Karachentsev, V. E. Karachentseva, and Y. N. Kudrya, *Astrophysical Bulletin* **71** (2), 129 (2016).  
 I. D. Karachentsev and Y. N. Kudrya, *Astron. J.* **148** (3), 50 (2014).  
 I. D. Karachentsev and D. I. Makarov, *Astrophysical Bulletin* **63** (4), 299 (2008).  
 V. E. Karachentseva, I. D. Karachentsev, and O. V. Melnyk, *Astrophysical Bulletin* **76** (4), 341 (2021).  
 A. Koch and E. K. Grebel, *Astron. J.* **131** (3), 1405 (2006).  
 D. M. Koranyi and M. J. Geller, *Astron. J.* **123** (1), 100 (2002).  
 E. Kourkchi and R. B. Tully, *Astrophys. J.* **843** (1), article id. 16 (2017).  
 P. Kroupa, C. Theis, and C. M. Boily, *Astron. and Astrophys.* **431**, 517 (2005).  
 N. I. Libeskind, E. Carlesi, O. Müller, et al., *Monthly Notices Royal Astron. Soc.* **490** (3), 3786 (2019).  
 D. Makarov and I. Karachentsev, *Monthly Notices Royal Astron. Soc.* **412** (4), 2498 (2011).  
 D. Makarov, P. Prugniel, N. Terekhova, et al., *Astron. and Astrophys.* **570**, id. A13 (2014).  
 D. Makarov, S. Savchenko, A. Mosenkov, et al., *Monthly Notices Royal Astron. Soc.* **511** (2), 3063 (2022).

D. I. Makarov and I. D. Karachentsev, *Astrophysical Bulletin* **64** (1), 24 (2009).

D. I. Makarov and R. I. Uklein, *Astrophysical Bulletin* **67** (2), 135 (2012).

D. Martínez-Delgado, D. Makarov, B. Javanmardi, et al., *Astron. and Astrophys.* **652**, id. A48 (2021).

M. J. Meyer, M. A. Zwaan, R. L. Webster, et al., *Monthly Notices Royal Astron. Soc.* **350** (4), 1195 (2004).

M. S. Pawlowski, B. Famaey, D. Merritt, and P. Kroupa, *Astrophys. J.* **815** (1), article id. 19 (2015).

M. Ramella, M. J. Geller, A. Pisani, and L. N. da Costa, *Astron. J.* **123** (6), 2976 (2002).

E. F. Schlafly and D. P. Finkbeiner, *Astrophys. J.* **737** (2), article id. 103 (2011).

K. Shimasaku, M. Fukugita, M. Doi, et al., *Astron. J.* **122** (3), 1238 (2001).

M. F. Skrutskie, R. M. Cutri, R. Stiening, et al., *Astron. J.* **131** (2), 1163 (2006).

J. L. Tonry, C. W. Stubbs, K. R. Lykke, et al., *Astrophys. J.* **750** (2), article id. 99 (2012).

R. B. Tully, *Astrophys. J.* **618** (1), 214 (2005).

R. B. Tully, N. I. Libeskind, I. D. Karachentsev, et al., *Astrophys. J.* **802** (2), article id. L25 (2015).

R. B. Tully, L. Rizzi, A. E. Dolphin, et al., *Astron. J.* **132** (2), 729 (2006).

M. Viola, M. Cacciato, M. Brouwer, et al., *Monthly Notices Royal Astron. Soc.* **452** (4), 3529 (2015).

R. H. Wechsler and J. L. Tinker, *Annual Rev. Astron. Astrophys.* **56**, 435 (2018).

D. Zaritsky, R. Smith, C. Frenk, and S. D. M. White, *Astrophys. J.* **405**, 464 (1993).

D. Zaritsky, R. Smith, C. Frenk, and S. D. M. White, *Astrophys. J.* **478** (1), 39 (1997).

D. Zaritsky and S. D. M. White, *Astrophys. J.* **435**, 599 (1994).

A. V. Zasov, A. S. Saburova, A. V. Khoperskov, and S. A. Khoperskov, *Physics Uspekhi* **60** (1), 3 (2017).

H. Zou, X. Zhou, X. Fan, et al., *Astrophys. J. Suppl.* **245** (1), article id. 4 (2019).

## APPENDIX A

### GALAXIES EXCLUDED FROM CONSIDERATION

Information about the membership of galaxies in clusters and their radial velocities was taken from the HyperLeda (Makarov et al., 2014) database.

- SDSS J000301.88+331036.1, a candidate

- satellite of EGIPS J000312.06+331118.0, projects close to the tight pair SDSS J000302.29+331032.6 and SDSS J000302.15+331024.6, which are part of a galaxy cluster. With the exception of the EGIPS galaxy and the candidate satellite, redshift measurements are unavailable for the remaining cluster members; however, evidently, the cluster is real and these two galaxies are its members.
- PGC 1157067 and its main galaxy EGIPS J011551.3+000848 are located at the periphery of the ABELL 168 cluster. The radial velocity relative to the cluster center is approximately  $1700 \text{ km s}^{-1}$ .
  - EGIPS J030718.3–093645 (NGC 1216) and its candidate satellite HCG 023:[dRC97]26 are, probably, members of a compact HCG023 (Hickson, 1982) group. Their radial velocities differ from the group velocity by 775 and  $685 \text{ km s}^{-1}$  correspondingly.
  - The EGIPS J031922.9+004924 galaxy and its candidate satellites SDSS J031844.25+005302.5 and PGC 1176312 are excluded from consideration due to a possible connection with the [BFW2006] MR18\_06184 group with a radial velocity of  $10949 \text{ km s}^{-1}$ .
  - As is evident in the image, the EGIPS J074900.3+370942 galaxy (with PGC 3128739 as its candidate satellite) is interacting with a close companion, PGC 021876, which has no redshift data. The magnitude difference is less than  $1^m$ , so the system should not have passed the second stage of selection.
  - EGIPS J075939.3+263309 and its candidate satellite PGC 1781379 are located at the periphery of the IC 486, IC 485, IC 484 group. We excluded it from consideration to avoid the edge effects, despite the rather large velocity difference of  $672 \text{ km s}^{-1}$ .
  - The EGIPS J080613.4+174223 (NGC 2522) with all its candidates satellites—PGC 1534373, PGC 1536557, SDSS J080627.26+174317.1 and PGC 1548640—are members of the

USGC U167 (Ramella et al., 2002) group. It was missed by the selection algorithm due to the velocity difference between EGIPS J080613.4+174223 and the other known companions of the USGC U167 group of over  $300 \text{ km s}^{-1}$ .

- A sparse structure of galaxies is observed in the direction of EGIPS J104046.9–090040 and its candidate satellite PGC 996238 with a radial velocity of  $9000 \text{ km s}^{-1}$ , close to the velocity of the pair of galaxies under consideration. The ABELL 1069 cluster is located in the background.
- The image shows that EGIPS J155604.4+402747 (its candidate satellite is SDSS J155543.93+402703.8) is interacting with a close brighter companion, SDSS J155605.25+402752.8, with no redshift measurements available. As a consequence, the pair was missed by the algorithm.
- The central object EGIPS J160459.5+235812, with PGC 2567181 as a candidate satellite, is a member of the AWM 4 (Koranyi and Geller, 2002) cluster. The radial velocity difference of  $1719 \text{ km s}^{-1}$  turned out to be too large for an association of the EGIS galaxy with the cluster by our algorithm.
- EGIPS J161234.0+253002 (its candidate satellite is SDSS J161155.08+253725.8) possibly forms a group with SDSS J161212.79+253340.3, which is a spiral galaxy of comparable luminosity. Only the photometric redshift is known for the latter,  $z_{\text{photo}} = 0.033$  (Bilicki et al., 2014), which does not contradict the suggestion that they form a bound system with the EGIPS J161234.0+253002 galaxy.
- EGIPS J171524.2+572101 (NGC 6345) and its candidate satellite PGC 2567181 were excluded due to a possible connection to the group of galaxies around NGC 6338, despite the  $1737 \text{ km s}^{-1}$  radial velocity difference.
- An XLSB galaxy PGC 3441769 of comparable size is projected onto the central galaxy EGIPS J225650.8–085803 (its candidate satellite is PGC070056). The galaxies likely

form a close pair.

- EGIPS J234800.6+272231 together with its candidate satellites PGC 1809943 and PGC 085775 are located at the periphery of the ABELL 2666 cluster. The radial velocity relative to the cluster center is  $480 \text{ km s}^{-1}$ .